Science of the Total Environment 867 (2023) 161365

Contents lists available at ScienceDirect

Science of the Total Environment

journal homepage: www.elsevier.com/locate/scitotenv

A spatial fingerprint of land-water linkage of biodiversity uncovered by remote sensing and environmental DNA

Heng Zhang [a,b,*], Elvira Mächler [a,b], Felix Morsdorf [c], Pascal A. Niklaus [a], Michael E. Schaepman [c], Florian Altermatt [a,b,*]

[a] Department of Evolutionary Biology and Environmental Studies, University of Zurich, Winterthurerstrasse 190, CH-8057 Zürich, Switzerland
[b] Eawag, Swiss Federal Institute of Aquatic Science and Technology, Department of Aquatic Ecology, Überlandstrasse 133, CH-8600 Dübendorf, Switzerland
[c] Remote Sensing Laboratories, Department of Geography, University of Zurich, Winterthurerstrasse 190, CH-8057 Zürich, Switzerland

HIGHLIGHTS

- Combining Sentinel-2 and eDNA data reveals a land-water linkage of biodiversity.
- The spatial range of this linkage extends up to 2 km.
- Vegetation functional diversity is the dominant contributor to this linkage.
- The biodiversity signal detected contains aquatic and terrestrial organisms.

GRAPHICAL ABSTRACT

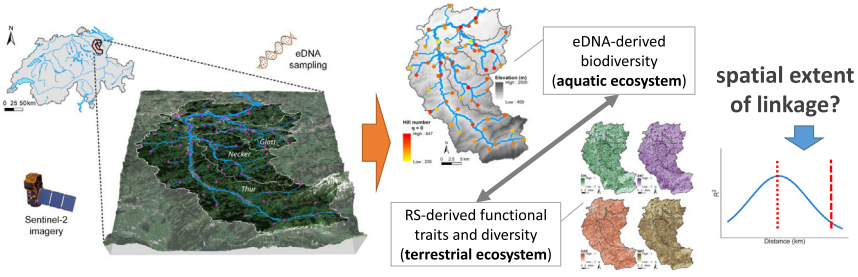

ARTICLE INFO

Editor: Sergi Sabater

Keywords:
Biodiversity
Remote sensing
Functional trait
Environmental DNA

ABSTRACT

Aquatic and terrestrial ecosystems are tightly connected via spatial flows of organisms and resources. Such land-water linkages integrate biodiversity across ecosystems and suggest a spatial association of aquatic and terrestrial biodiversity. However, knowledge about the extent of this spatial association is limited. By combining satellite remote sensing (RS) and environmental DNA (eDNA) extraction from river water across a 740-km^2 mountainous catchment, we identify a characteristic spatial land-water fingerprint. Specifically, we find a spatial association of riverine eDNA diversity with RS spectral diversity of terrestrial ecosystems upstream, peaking at a 400 m distance yet still detectable up to a 2.0 km radius. Our findings show that biodiversity patterns in rivers can be linked to the functional diversity of surrounding terrestrial ecosystems and provide a dominant scale at which these linkages are strongest. Such spatially explicit information is necessary for a functional understanding of land-water linkages.

1. Introduction

Understanding the spatial distribution of biodiversity and its linkage across ecosystem types is essential, especially in an era of increasing human modifications of natural landscapes (Kennedy et al., 2019; Pimm et al., 2014). It is well-established that species and ecosystem functional diversity are unevenly distributed across landscapes, with pronounced diversity hot and cold spots (Hughes et al., 2021; Mittermeier et al., 2011). Intriguingly, however, most past work has focused on individual ecosystem types, such as forests, grasslands, or aquatic ecosystems, thereby neglecting a possible co-variation of biodiversity across different ecosystems. Indeed, only very recently the relevance of spatial scaling of biodiversity and ecosystem functioning research and the dependence on the spatial extent has been postulated (Gonzalez et al., 2020; Thompson et al., 2021).

Natural ecosystems, and the biodiversity therein, are often linked to each other through flows of organisms and resources (Gounand et al., 2018a; Guichard and Marleau, 2021; Loreau et al., 2003). One of the most prominent examples is the coupling of aquatic to terrestrial ecosystems (Gounand et al., 2018b; Grimm et al., 2003; Soininen et al., 2015).

* Corresponding authors at: Department of Evolutionary Biology and Environmental Studies, University of Zurich, Winterthurerstrasse 190, CH-8057 Zürich, Switzerland.
E-mail addresses: Heng.Zhang@eawag.ch (H. Zhang), Florian.Altermatt@ieu.uzh.ch (F. Altermatt).

http://dx.doi.org/10.1016/j.scitotenv.2022.161365
Received 14 September 2022; Received in revised form 6 December 2022; Accepted 30 December 2022
Available online 10 January 2023

Aquatic ecosystems are not only highly biodiverse yet threatened by anthropogenic activities (Dudgeon, 2019), but also strongly influenced by surrounding terrestrial ecosystems through the characteristic fractal structure of riverine networks embedded across most landscapes worldwide (Dahlin et al., 2021; Gounand et al., 2018b; Rodriguez-Iturbe and Rinaldo, 2001). Consequently, in these connected systems, a characteristic in one ecosystem resulting in an imprint on the diversity of the other ecosystem is expected, with implications for land management and conservation (Polis et al., 1997). Specifically, in the aquatic-terrestrial linkage, a site in the river and its terrestrial vicinity area are tightly shaped by a dominant impact direction from terrestrial to aquatic ecosystems. Multiple mechanisms, such as direct effect of organismal movement (Ward et al., 2002), and indirect effects of resource subsidies (Gravel et al., 2010) and food web interactions (Leroux and Loreau, 2008; Nakano and Murakami, 2001), have been hypothesized to explain such cross-ecosystem interactions. For instance, animal movements across landscapes can, at the same time, alter carbon exchange and storage, transport of nutrients, and trophic cascades (Polis et al., 1997; Schmitz et al., 2018). While proposed individually, all these mechanisms are essentially mutually non-exclusive, and the differentiation into them requires manipulative studies. Nevertheless, little is known about the spatial extent of such a linkage, particularly regarding the spatial range at which one ecosystem could influence local biodiversity in the respective other ecosystems. Such information, however, is crucial because the spatial extent of linkage of biodiversity across ecosystems, generating a “spatial fingerprint”, can be seen as a basic unit at which biodiversity in the river is significantly influenced by the surrounding terrestrial ecosystems, or in other words, where the linkage of ecosystems modulates local biodiversity. The concept of such a spatial fingerprint of land-water linkage of biodiversity enables analyzing biodiversity patterns at the catchment level. In addition, the spatial extent itself has potentially a broad meaning because it provides not only a spatial extent for local cross-ecosystem linkage of biodiversity, but also a reference scale for aquatic biodiversity protection in terms of surrounding terrestrial land use management.

In natural ecosystems, higher landscape richness, or more directly landscape heterogeneity, can promote biodiversity and ecosystem functioning at the local scale (Oehri et al., 2020). Moreover, spatial flows of resources and organisms drive a land-water linkage of organisms and resources in a catchment (Gravel et al., 2010; Ward et al., 2002). This allows the formulation of the core hypothesis of this study, which is the existence of the land-water (cross-ecosystem) linkage of biodiversity, herein termed as the spatial fingerprint of land-water linkage. Following this, our second hypothesis focuses on the dominant scale of the spatial fingerprint. We assume that the spatial association between terrestrial ecosystem functioning and the diversity of riverine communities would maximize where local heterogeneity of terrestrial landscape and spatial flows of resources and organisms are mostly integrated, but would then decrease with increasing distances. Furthermore, we also hypothesize that the indirect effects mostly, but not exclusively, contribute to the land-water linkage of biodiversity.

To testify to these hypotheses and quantify the spatial extent of linkage of diversity across ecosystem types, biodiversity must be quantified in scalable and comparable manners. Classically, biodiversity is directly quantified by counting individual species, for example, through inventories conducted along transects or in plots of defined size. This approach, however, has inherent limitations for spatial upscaling and cross-ecosystem comparisons (Gonzalez et al., 2020). Currently, two recent technological advances are revolutionizing biodiversity sciences, overcoming limitations with taxonomic and functional coverage, and the possibility to be spatially scaled. The first advancement is through remote sensing (RS) methods, which use portable, airborne, or satellite devices to characterize the ecosystem structurally, taxonomically, or physiologically by measuring reflected or emitted radiation at a distance (O'Connor et al., 2020; Pereira et al., 2013; Skidmore et al., 2021). RS is particularly capable of characterizing terrestrial plant communities and a prime method for measuring essential biodiversity variables (EBVs) (O'Connor et al., 2020; Pereira et al., 2013; Skidmore et al., 2021). Particularly, RS can map terrestrial ecosystem functional traits and diversity at regional to global scales with resolutions down to a meter, enabling the upscaling of biodiversity from local composition to ecosystem levels (Jetz et al., 2016; Schneider et al., 2017; Zheng et al., 2020). The second advancement is through environmental DNA (eDNA) metabarcoding. It is based on the finding that organism's occurrence can be inferred from environmental samples containing their DNA. This DNA can be collected, sequenced and matched to taxonomic databases in a standardized and quantitative manner, making biodiversity assessment more accurate and efficient (Cilleros et al., 2019; Lodge et al., 2012; Taberlet et al., 2012; Thomsen and Willerslev, 2015). In aquatic biodiversity surveys, eDNA metabarcoding is so powerful that organismal communities can be reconstructed from a few liters of water, drastically transforming how microbial and macrobial communities are surveyed (Keck et al., 2022). Therefore, this new technology is widely used in aquatic ecosystem studies, and it is becoming a standard for aquatic biodiversity assessments (Bista et al., 2017; Bohmann et al., 2014; Deiner et al., 2017; Turak et al., 2017). The passive transport of DNA in water makes it a particularly efficient method in riverine systems, as the flow along the riverine network carries and integrates biodiversity information over the catchment (Deiner et al., 2016; Pont et al., 2018; Shogren et al., 2017), and can be used for estimating spatial patterns of biodiversity at the landscape level (Carraro et al., 2020; Shackleton et al., 2019).

Essentially, RS and eDNA metabarcoding complement each other in biodiversity detection. RS is especially powerful in monitoring terrestrial ecosystems, including physiological properties and structural diversity of vegetation. Contrastingly, environmental DNA is especially powerful in assessing biodiversity in riverine systems, including microbial organisms, invertebrates, and vertebrates, which are largely inaccessible for RS. Therefore, a combination of RS for terrestrial ecosystems and eDNA for aquatic ecosystems can provide a holistic view of biodiversity for spatially coupled ecosystems (Lausch et al., 2018; Yamasaki et al., 2017). Most importantly, it allows uncovering the spatial scale of land-water linkages of biodiversity at the landscape level (Bush et al., 2017; Lin et al., 2021).

Here, we quantified the spatial extent of a linkage of biodiversity between aquatic and terrestrial ecosystems by combining RS and eDNA sampling in a 740-km^2 river drainage basin to testify to the hypotheses mentioned above. We assessed aquatic biodiversity of a broad range eukaryotic microorganisms, macro- and micro-invertebrates, and vertebrates along the river network using a generic marker covering a wide breadth of taxa. Then, we matched the eDNA-derived aquatic biodiversity to terrestrial ecosystem functional diversity in the catchment based on Sentinel-2 MultiSpectral Instrument (MSI) satellite data. Specifically, as for the first and second hypotheses, we identified the spatial range within which the functional diversity of the terrestrial vegetation was associated with the taxonomic diversity in the riverine ecosystems and determined at what spatial scale this linkage was the highest. We then tested our third hypothesis of possible mechanisms with respect to direct or indirect effects. Thereby, combining RS and eDNA, we provide a first spatially explicit integration of land-water linkage of biodiversity, and identify a characteristic spatial fingerprint across aquatic-terrestrial ecosystem boundaries at the landscape level.

2. Methods

We combined assessments of aquatic biodiversity using eDNA and terrestrial diversity based on Sentinel-2 MSI satellite data in the 740 km^2 Thur river catchment (Fig. 1). The Thur river catchment is located in the northeastern part of Switzerland. It covers a mountainous landscape with an elevation gradient ranging from 460 m to 2423 m a.s.l. and contains a mosaicked landscape of urban, agricultural, and forested terrestrial ecosystem types.

2.1. RS-derived physiological traits and functional diversity in terrestrial ecosystems

2.1.1. Physiological traits in terrestrial ecosystems by Sentinel-2 MSI

Functional diversity metrics can provide essential information on terrestrial ecosystem functioning and are capable to be mapped from either

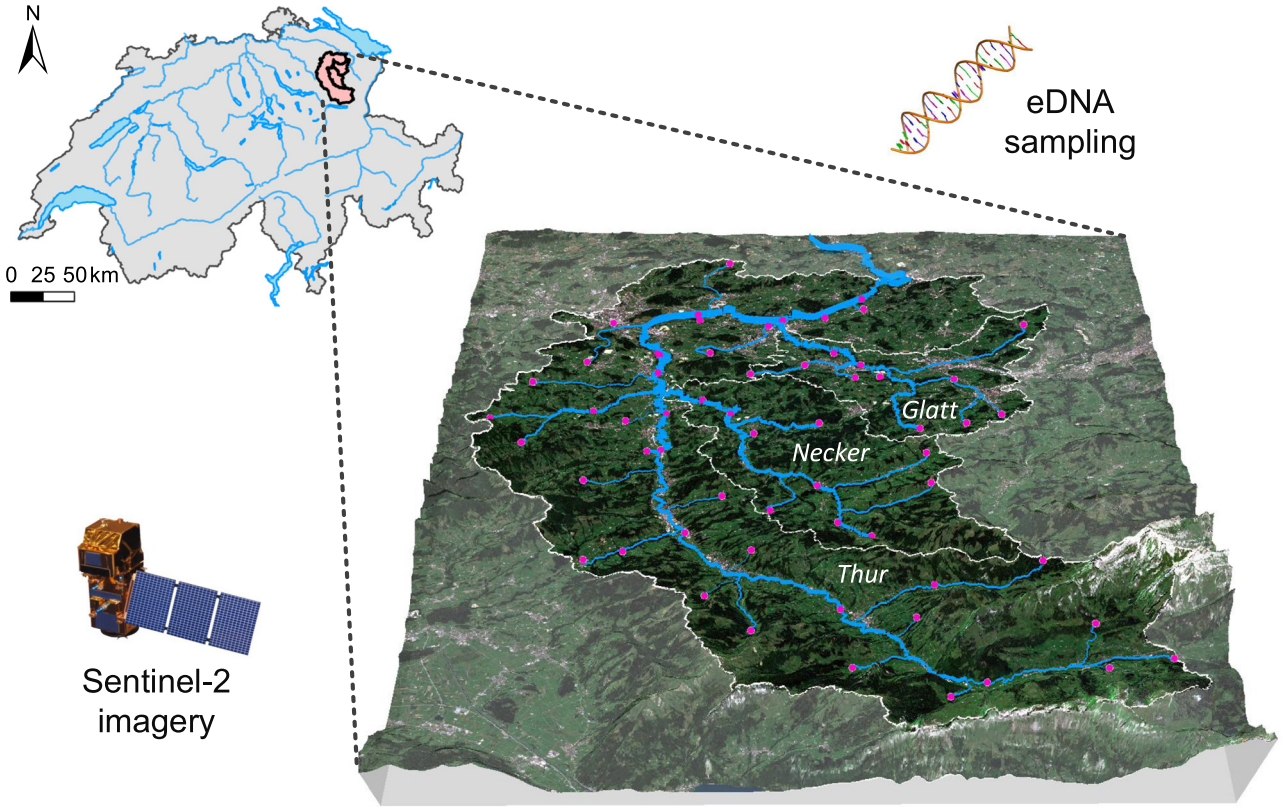

Fig. 1. Location of the Thur river catchment in Switzerland and eDNA sampling sites. Pink dots are 61 eDNA sampling sites. The blue lines represent river channels draining in a Northward direction. White lines indicate the boundaries of the main catchment and its three subcatchments (Thur, Necker, and Glatt).

airborne (Schneider et al., 2017) or satellite platforms (Helfenstein et al., 2022). With a resolution of 20 m and multi-spectral information covering large parts of the visible and near-infrared spectral domain, data from the Sentinel-2 satellites are particularly suited for monitoring physiological properties of terrestrial ecosystems. Thus, we adapted a spatially continuous method, which was generalized to Sentinel-2 MSI satellite data, to map the terrestrial ecosystem functional diversity (a metric in EBVs) at a 20 × 20 m resolution (Drusch et al., 2012; Helfenstein et al., 2022). With the multi-spectral data from Sentinel-2, one can estimate physiological traits of vegetation and their spatial variations through well-established vegetation indices (see Supplementary Text). Specifically, we selected vegetation indices that are linked to chlorophyll content (CHL), anthocyanin content (ANT), carotenoid content (CAR), and water content (WAT) to construct a four-dimensional trait space. Functionally, chlorophyll (green pigment) enables plants to capture energy from light in the photosynthesis reaction; anthocyanin (blue, red, and purple pigment) replaces chlorophyll during the leaf senescence process; carotenoid (orange and yellow pigment) prevents possible damage in stress conditions; water content reflects dry weight and drought stress among the plants (Jetz et al., 2016). Hence, such traits integrally represent the presence and conditions of vegetation and reflect the variation and spatial distribution of physiological traits of vegetation (Díaz et al., 2016).

All vegetation indices were computed on Google Earth Engine (GEE), a cloud-based platform for spatial analysis (Gorelick et al., 2017). We selected Sentinel-2 MSI Level-2A calibrated surface reflectance (SR) image collections between June and August in 2017, as no SR images were produced at the time of eDNA sampling. Based on a cloud-free image acquired by employing a median filter to the selected image collections, we calculated eleven spectra indices representing CHL, ANT, CAR, and WAT. All detailed formulas of these vegetation indices are shown in the Supplementary Text.

2.1.2. Selection of physiological traits

To reduce collinearity, we chose one vegetation-index-based trait proxy in each physiological trait dimension. We computed a correlation matrix of all the normalized physiological trait proxies (Fig. S1a) and enumerated all possible four-trait-proxy subsets. For each subset, we calculated the Frobenius norm ($\|\boldsymbol{A}\|_F$) of the correlation matrix ($\boldsymbol{A}$), according to Eq. (1).

$$\boldsymbol{A} = \begin{bmatrix} a_{11} & \cdots & a_{1n} \\ \vdots & \ddots & \vdots \\ a_{m1} & \cdots & a_{mn} \end{bmatrix}, \quad \|\boldsymbol{A}\|_F = \sqrt{\sum_{i=1}^{m}\sum_{j=1}^{n} |a_{ij}|^2}. \tag{1}$$

Next, we found an optimal subset with the lowest Frobenius norm (Fig. S1b). The selected trait proxies were CI_{re} (CHL), *ARI*1 (ANT), *PSRI* (CAR), and *NDII* (WAT). We observed less collinearity among the selected proxies except for CHL against WAT, where positive correlation is unavoidable because both trait proxies, though in different aspects, reflect the condition of vegetation photosynthesis (Fig. S2).

2.1.3. Terrestrial ecosystem functional diversity in the catchment across distance

We used the 25 × 25 m digital elevation model (DEM) of the study area provided by the Swiss Federal Institute of Topography (Swisstopo) to extract the catchment of each eDNA sampling site. ArcGIS software (version 10.3) was used to generate a flow direction map based on the DEM. We produced a catchment map with flow distance for each site by tracing the water flow direction of each pixel and recording its flow distance to the site. Upstream distance buffers of each sampling site were created by setting the spatial interval to 0.05 km for 0–10 km and 0.1 km for 10–20 km (Fig. 2).

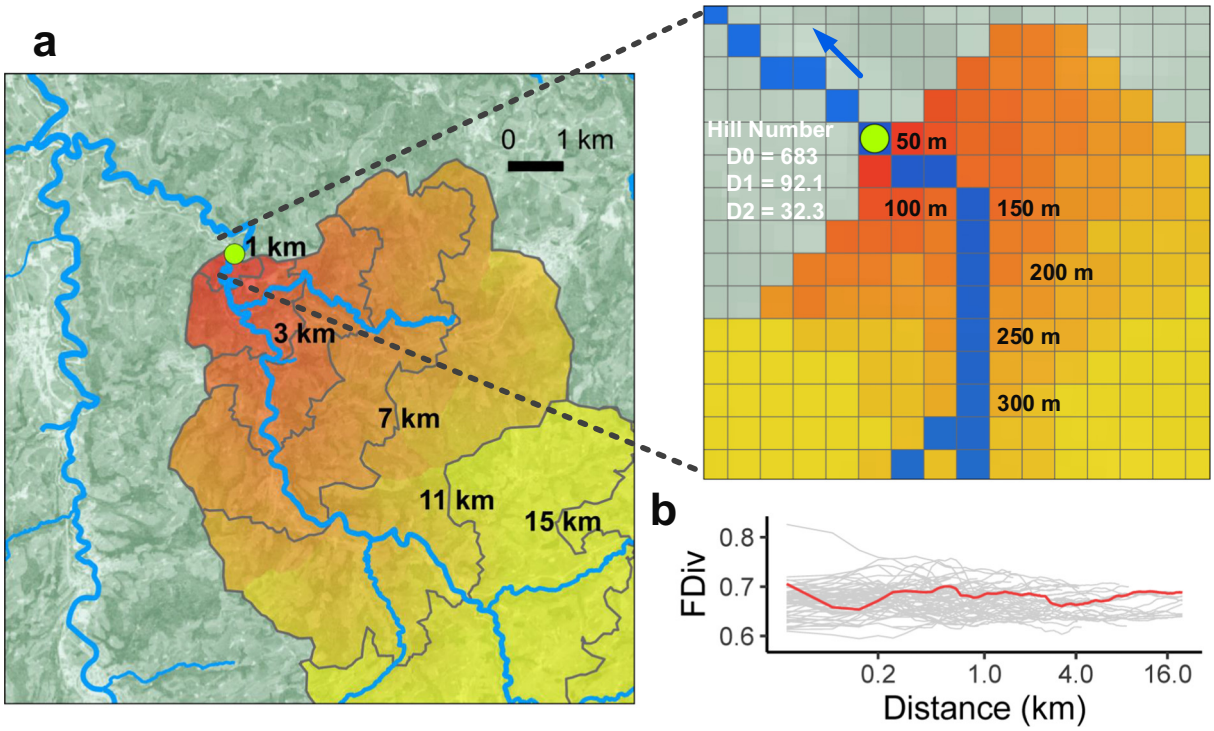

Fig. 2. Upstream distance buffers of the eDNA sampling site and terrestrial ecosystem functional diversity based on these distance buffers. **a**. Catchment map with distance buffers (1 km, 3 km, etc.) of site No. 29 as an example. Flow distance for each pixel was calculated by tracing the 25 × 25 m flow direction map. Colors from red to yellow indicate the increasing trend of flow distance. The zoom-in figure represents the 50 m spatial interval for distance buffers (color scale adjusted). **b**. Functional divergence (FDiv) with upstream distance given for 61 eDNA sampling sites (grey lines; the example site No. 29 is highlighted as red line). We calculated FDiv by collecting four-dimensional trait value vectors from pixels covered by the distance buffer. Non-vegetated pixels were masked out before computation.

We chose functional divergence (FDiv) among three types of functional diversity metric (functional richness, functional divergence, and functional evenness) because FDiv best captured the variation of terrestrial ecosystem functions and was the most robust to noise and outliers (Schneider et al., 2017; Villéger et al., 2008). For each sampling site with an upstream distance buffer, based on the normalized selected trait proxies, we extracted four-dimensional trait proxy value vectors (V_i) from vegetated pixels (i = 1, 2, …, s) that covered by the upstream distance buffer and calculated FDiv by following Eqs. (2)–(5).

$$C = \frac{1}{s}\sum_{i=1}^{s} V_i. \tag{2}$$

$$dG_i = \|V_i - C\|_2 \tag{3}$$

$$\Delta|d| = \frac{1}{s}\sum_{i=1}^{s}|dG_i - \overline{dG}| \tag{4}$$

$$\mathrm{FDiv} = \frac{\overline{dG}}{\Delta|d| + \overline{dG}} \tag{5}$$

s is the number of vegetated pixels in the upstream distance buffer; C is the center of gravity of all vectors; dG_i is the Euclidean distance between the vector of i^{th} pixel (V_i) and the center of gravity (C). $\overline{dG}$ is the mean Euclidean distance of all vectors to C. In a special case, FDiv equals to 1 if all pixels are in a perfect sphere with equal distance to C.

2.2. eDNA-derived biodiversity in aquatic ecosystem

2.2.1. eDNA sampling in the Thur river network

The Thur catchment covers an area of 740 km^2 with three main river branches (Thur, Glatt, and Necker) and the main land covers including forest (29.0 %), arable and grassland (56.0 %), urban area (10.2 %), unproductive land (3.6 %), and water (1.2 %) land types (data from Swiss Federal Statistical Office, 2015. website: https://www.bfs.admin.ch/bfs/en/home/services/geostat/swiss-federal-statistics-geodata/land-use-cover-suitability/swiss-land-use-statistics/land-use.html). A systematic eDNA sampling was conducted in June 2016 under base-flow conditions. The detailed sampling, laboratory work, and subsequent bioinformatic analyses followed established standard procedures are described in Mächler et al. (2019, 2021), who analyzed the diversity of a small subset of all organisms and established methodological protocols for the eDNA sampling, respectively. In total, we collected 183 water samples at 61 sites (three individual replicates per site) in the dendritic river network. For each replicate, 250 ml of river water was filtered on site using GF/F filters (pore size 0.7 μm Whatman International Ltd.), and the filters were then immediately stored at −20 °C. Subsequently, DNA was extracted in a specifically dedicated clean lab, using the DNeasy Blood and Tissue Kit (Qiagen GmbH). Handling and extraction of all replicates were done in a randomized order. We performed two PCR runs with the Illumina MiSeq dual-barcoded two-step PCR amplicon sequencing protocol by targeting a short barcode region of the cytochrome *c* oxidase I (COI), covering a wide breadth of taxa including eukaryotic microorganisms, macro- and micro-invertebrates, and vertebrates (Leray et al., 2013). We used a two-step PCR approach: The first step covered 44 cycles where we used primers containing an Illumina adaptor-specific tail, a heterogeneity spacer, and the amplicon target site. The second step covered 10 cycles only and contained the Nextera XT Index Kit v2 for indexing, thereby reducing tag switches due to PCR errors. Filter controls (FC), extraction controls (EC), positive and negative PCR controls (PC, NC) were run alongside. The sequence data were subsequently demultiplexed, and the quality of the reads was checked with FastQC (Andrews, 2010). Then, we end-trimmed (usearch, version 10.0.240), merged the raw reads (Flash, version 1.2.11), removed primer sites (cutadapt, version 1.12), and quality-filtered the data (prinseq-lite,

version 0.20.4). Next, we used UNOISE3 (usearch, version 10.0.240) to determine ZOTUs, and performed an additional clustering at 99 % sequence identity to reduce sequence diversity. Before final use, the resulting ZOTUs were checked for stop codons with invertebrate mitochondrial code, and to only contain an intact open reading frame.

We merged the ZOTU abundances of the three replicates at each site and obtained 26,519,031 reads clustered into 10,962 ZOTUs. Then, we calculated the relative abundance for each ZOTU at all sampling sites. To alleviate uncertainties, we filtered out the ZOTUs with <0.005 % occurrence in total (i.e., <1326 total reads) and finally used 24,471,930 reads clustered into 1394 ZOTUs for all analyses (2404 ± 216 (mean ± standard error) number of reads per ZOTU). Taxonomic information at the phylum and the class level for all ZOTUs was acquired by mapping against a customized MIDORI Reference 2 (UNIQ/GB242) database. After that, we computed relative abundance for each ZOTU at each site with the number of reads of one ZOTU divided by total number of reads at one site (for a depiction of read-distribution across samples, see Fig. S3), subsequently referred to as our eDNA data.

2.2.2. Hill numbers as metrics of eDNA-derived biodiversity

We focus on richness and evenness-based descriptors of diversity, as these are most commonly used in biodiversity sciences. To describe different aspects of biodiversity across all eDNA samples, we used Hill numbers, which are a compatible statistical framework considering both occurrence and abundance information (Alberdi and Gilbert, 2019; Hill, 1973; Jost, 2007; Mächler et al., 2021). In this framework, the abundant species (with high ZOTU reads) enlarge their weights with increasing Hill number q orders. Though in different formulas, these metrics are directly relevant to some popular measurements of biodiversity. For instance, Hill numbers with order q = 0, 1, and 2 correspond to species richness, the exponential of Shannon diversity, and the inverse of the Simpson index, respectively. Therefore, to keep a consistency with these commonly used measurements, we calculated Hill numbers with order q = 0, 1, and 2 (Eqs. (6)–(7)) after removing very rare ZOTUs (occurrence < 0.005 % across the total 183 samples). For q = 1, Eq. (7) was used because it is the limit of Eq. (6) as q approaches one.

$$ {}^{q}D = \left(\sum_{i=1}^{s} p_i^q\right)^{1/(1-q)}, (q \neq 1). \tag{6} $$

$$ {}^{1}D = \exp\left(-\sum_{i=1}^{s} p_i \cdot \ln p_i\right), (q = 1). \tag{7} $$

s is the number of ZOTUs at each site, p_i is the relative abundance of ZOTU i.

2.3. Assessing associations of land-water linkage of biodiversity

2.3.1. Linear regression model to assess the strength and uncertainty of the linkage

Due to uncertainties in both eDNA and RS measurements, we employed a model II linear regression to assess the association between eDNA-derived biodiversity (Hill numbers) and the RS-derived terrestrial ecosystem functional diversity (FDiv) across distance upstream, using R^2 as the goodness of fit. As distance increased, sampling sites were removed from the regression model if their catchments were already entirely covered by the upstream distance buffer (Fig. S4). To estimate uncertainties, we subsampled 70 % of the available sampling sites 1000 times to build subsampling models, and then calculated the standard deviation of all R^2 results. The percentages of subsampling models with p-value < 0.05 are shown in Fig. S5.

2.3.2. Null models for comparison

We developed null models to ensure that the spatial association between aquatic and terrestrial ecosystems was not a measurement artifact. Specifically, the spatial location of pixels (with their respective functional trait measurement) within the river catchment was randomly shuffled in space 1000 times, followed by calculating FDiv for each sampling site according to the same upstream distance buffers generated before. Then, model II simple linear regression was performed to evaluate the correlation between the eDNA data and the shuffled RS data.

2.3.3. Evaluation of contributions of vegetation productivity and terrestrial ecosystem functional diversity

We calculated the enhanced vegetation index (EVI, Eq. (8)), which can be used to estimate vegetation productivity (Jiang et al., 2008; Sims et al., 2006). The EVI values were averaged across the upstream distance buffers after excluding non-vegetated pixels.

$$ \begin{aligned} EVI &= 2.5 \cdot \frac{\rho_{785-900} - \rho_{650-680}}{\rho_{785-900} + 6 \cdot \rho_{650-680} - 7.5 \cdot \rho_{458-523} + 1} \\ &= 2.5 \cdot \frac{B8 - B4}{B8 + 6 \cdot B4 - 7.5 \cdot B2 + 1} \end{aligned} \tag{8} $$

Then, we used linear models summarized in ANOVA tables with sequential (type I) tests to evaluate the relative contributions of EVI and FDiv to the Hill numbers (Hill) across distance, by Eqs. (9)–(10).

$$ \text{Test 1} : ANOVA(Hill \sim EVI + FDiv + EVI \times FDiv). \tag{9} $$

$$ \text{Test 2} : ANOVA(Hill \sim FDiv + EVI + FDiv \times EVI). \tag{10} $$

$EVI \times FDiv$ and $FDiv \times EVI$ are interaction terms.

2.4. Spatial autocorrelation in terrestrial ecosystem and the riverine network

Spatial autocorrelation is an intrinsic property of natural landscapes. The issue of spatial autocorrelation is relevant when the scale of distribution of sampling sites coincides with this inherent spatial property, thus affecting the sampling result pattern. Here, we used the empirical semivariogram ($\hat{\gamma}(h)$, namely the Matheron's estimator, see Eq. (11)), a statistic to display the variability between data points as a function of distance, to assess spatial autocorrelations in aquatic and terrestrial ecosystems (Matheron, 1963).

$$ \hat{\gamma}(h) = \frac{1}{2N(h)} \sum_{(i,j) \in \boldsymbol{J}_{h \pm \delta}} \left(Z(\boldsymbol{s}_i) - Z(\boldsymbol{s}_j)\right)^2. \tag{11} $$

$\boldsymbol{s}_i, \boldsymbol{s}_j$ are locations in the study area D. $\boldsymbol{J}_{h \pm \delta} = \{(i,j) : h - \delta \leq \|\boldsymbol{s}_i - \boldsymbol{s}_j\| < h + \delta; \boldsymbol{s}_i, \boldsymbol{s}_j \in D\}$ is the set of location pairs with a distance lag h, whose pairwise distances are in the range of $h \pm \delta$. $N(h) = |\boldsymbol{J}_{h \pm \delta}|$ is the number of location pairs in $\boldsymbol{J}_{h \pm \delta}$. $Z(\boldsymbol{s})$ is the spatial data (eDNA or RS data).

We conducted a spatial autocorrelation analysis for terrestrial pixels by calculating the empirical semi-variograms based on the four physiological trait proxies. We repeated the computation 300,000 times for each trait proxy map by randomly selecting two pixels within a Euclidean distance of 4 km and calculating the variance of trait values after removing non-vegetated pixels. Then, we calculated the $\hat{\gamma}(h)$ with binned distance (bin length = 0.025 km). We further fitted an exponential semi-variogram model, which is specified below.

$$ \gamma(h) = b + C_0 \cdot \left(1 - e^{-\frac{3h}{r}}\right). \tag{12} $$

Whereby r is the effective range. b is the nugget, the value at distance zero describing non-spatial variance. C_0 is the sill of semi-variogram, where the curve will level out and never be higher than $b + C_0$.

Following Eq. (11), we also calculated an empirical semi-variogram of the eDNA-derived biodiversity pattern (Hill number order q = 0) in our 61 sampling sites according to river channel structure, in which, for each site, only other sites upstream were used in the calculation. We binned the flow distance of point pairs with an interval of 0.025 km (h = 0.025,

0.050, …, 10 km; δ = 0.0125 km) to match the resolution of RS and DEM data, and then calculated the empirical semi-variogram.

3. Results

Based on the cloud-free Sentinel-2 MSI Level-2A SR data, we calculated spectral chlorophyll content (CHL), anthocyanin content (ANT), carotenoid content (CAR), and water content (WAT) to represent four physiological trait dimensions as direct proxies in functional diversity computation (Fig. 3; see Fig. S6 for density distributions). These spectral components capture plant physiological traits that integrate different components of terrestrial ecosystem functions, and thus functional diversity, related to the presence and conditions of vegetation (Fahey et al., 2019; Helfenstein et al., 2022). In the spatial autocorrelation analysis, we observed significant spatial autocorrelation patterns under all the four physiological trait proxies (CHL and WAT were strongest) and identified the effective range of spatial autocorrelation in terrestrial ecosystems to be 0.54–0.87 km (Fig. 3).

With the eDNA data, we calculated the eDNA-derived biodiversity in the riverine network with Hill number orders q = 0, 1, and 2, corresponding to species richness, the exponential of Shannon diversity, and the inverse of the Simpson index, respectively (Fig. 4). We observed strong and highly uneven biodiversity patterns across the catchment, with a strong and significant positive correlation between biodiversity and Strahler order (Fig. S7a–c; p-value < 0.05), and a decreasing trend of biodiversity at increasing elevation (Fig. S7d–f). We also simulated a spatial autocorrelation pattern using an exponential variogram model (Fig. S8b) and compared it with the empirical variogram plot of the eDNA data (Fig. S8a), where we added a local polynomial regression line as a reference. The result shows no significant spatial autocorrelation signal in our eDNA data, as there is no increasing trend at 0–4 km. In other words, we did not find an upstream spatial autocorrelation pattern in our 61 sampling sites.

The linear regression analysis reveals unimodal or bimodal associations between the eDNA-based (aquatic) Hill numbers and the RS-based (terrestrial) FDiv as the upstream distance to sampling sites increases, with a linkage signal covering an area of 1.0–1.7 km^2 up to 1.3–2.0 km radius upstream (Fig. 5). The distances with the highest R^2 (distance with maximal land-water association) vary across orders of q. For q = 0 (equivalent to species richness), this distance with the strongest association is 400 m, with a bootstrapped 90 % confidence interval (CI) of 350–1050 m; for q = 1 (equivalent to the exponential of Shannon diversity), it is 350 m (90 % CI: 150–400 m) and 850 m (90 % CI: 700–950 m), respectively; for q = 2 (equivalent to the inverse of Simpson index), it is 350 m (90 % CI: 200–500 m) and 850 m (90 % CI: 650–950 m), respectively. These results showing the existence and the spatial extent of land-water linkage of biodiversity testify to our first and second hypotheses. The strong effect of ZOTU-level richness decreases with increasing Hill number order (Fig. 5), suggesting that the occurrence of less abundant species has stronger association with FDiv, rather than the abundant species. Possibly, this could be ascribed to the decreasing contributions from the less abundant taxonomic groups after increasing the weight of abundance (increasing Hill number order q), as an abundant taxonomic group may swamp the effect of the less abundant ones. In addition, it highlights the importance of less abundant taxa contributing to overall beta-diversity (Kraft et al., 2011) and the negative effect of large-scale homogenization of biodiversity (Blowes et al., 2019), which results not only in an erosion of beta-diversity within one ecosystem but has also a cascading negative effect on other ecosystems. Given the strongest signal with Hill numbers of order q = 0, which is equivalent to species richness from presence-absence data and thus relatively conservative, we conclude that the spatial fingerprint of land-water linkage of biodiversity is robust. This is also in line with a broader body of evidence suggesting that eDNA based data are most robust for presence-absence data, yet may also capture abundance aspects especially for unicellular organisms or fish (Visco et al., 2015).

We developed null models to corroborate the robustness of linear models and to assess the maximal spatial extent of the land-water linkage, by randomly shuffling the locations of all pixels within the river catchment (Fig. S9). Then, we assessed whether and at what spatial extent such a land-water linkage of biodiversity exists in a null-model scenario. We found that the R^2 of our sampling was always greater than the null model for distances <2.0 km (90 % CI: 1.0–4.25 km) for q = 0 (species richness), <1.45 km

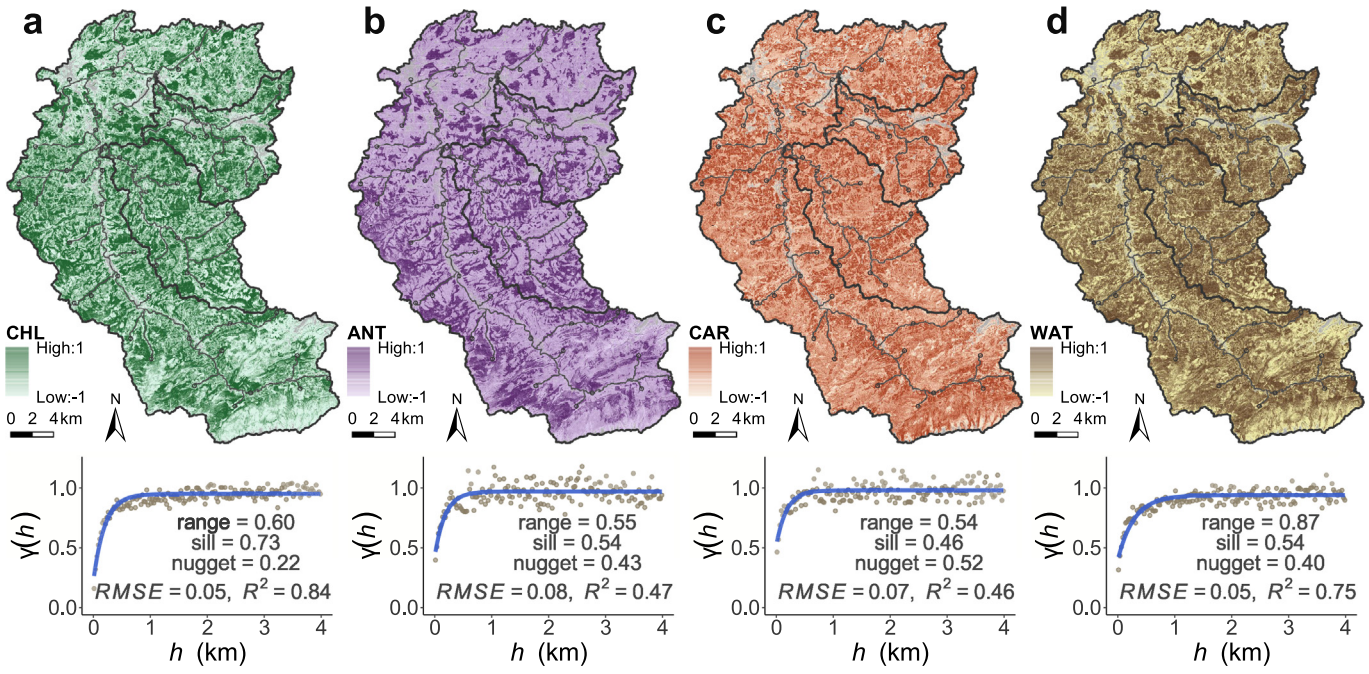

Fig. 3. Functional trait proxies assessed through physiological trait characteristics of the terrestrial landscape in the Thur river catchment. **a**. Map and semi-variogram plot of chlorophyll content (CHL), represented by the red-edge chlorophyll index (CI_{re}). **b**. Map and semi-variogram plot of anthocyanin content (ANT), represented by the anthocyanin reflectance index 1 (ARI1). **c**. Map and semi-variogram plot of carotenoid content (CAR), represented by the plant senescence reflectance index (PSRI). **d**. Map and semi-variogram plot of water content (WAT), represented by the normalized difference infrared index (NDII). Non-vegetated pixels were masked out (grey area), and all traits were normalized.

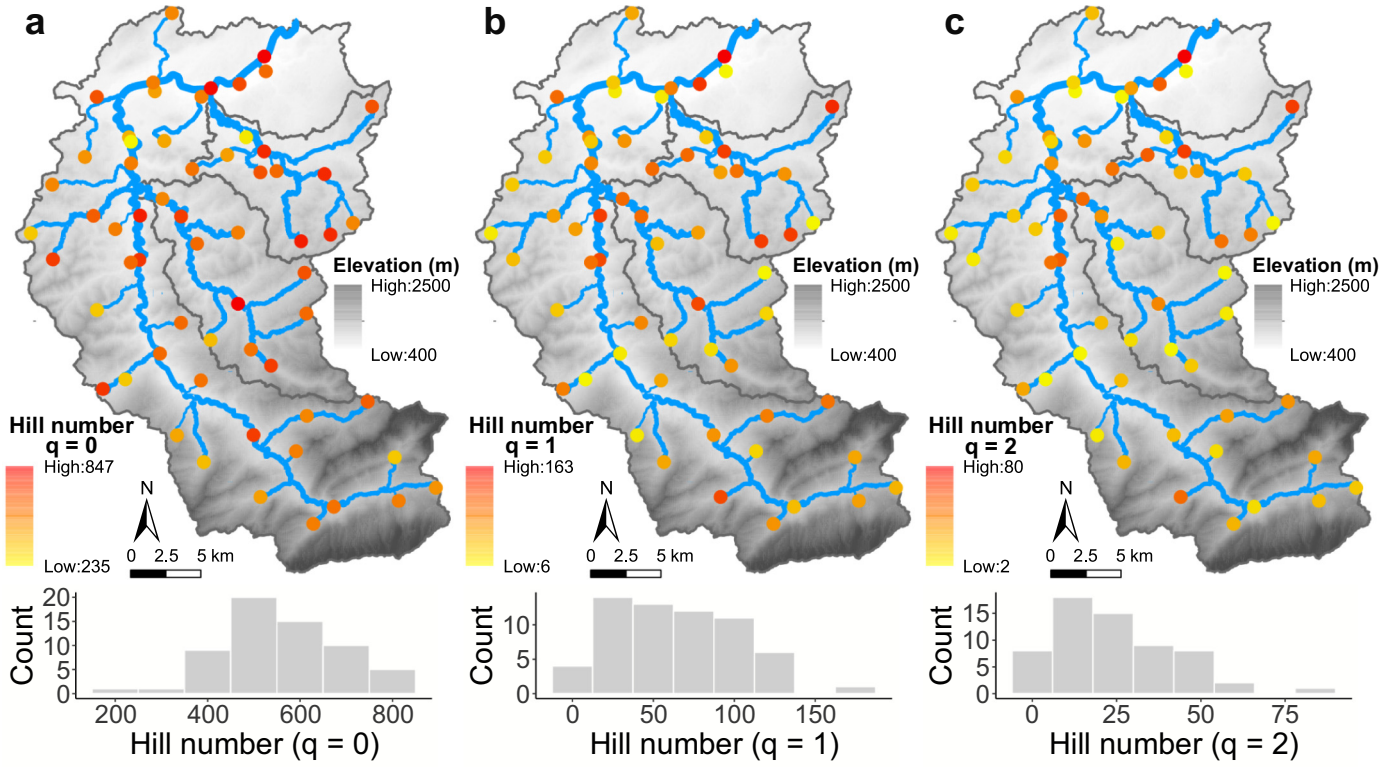

Fig. 4. Distribution of biodiversity in the river of the Thur river catchment. Hill numbers were used to describe biodiversity of eDNA samples in the river network. Spatial patterns and histograms on distribution of diversity using Hill numbers with order **a**. q = 0, **b**. q = 1, and **c**. q = 2 are given. They correspond to species richness (order q = 0), the exponential of Shannon diversity (order q = 1), and the Simpson index (order q = 2), respectively.

(90 % CI: 0.95–2.85 km) for q = 1 (the exponential of Shannon diversity), and <1.3 km (90 % CI: 0.95–4.05 km) for q = 2 (the inverse of Simpson index), respectively (Fig. 5). These results testify that biodiversity in riverine ecosystems can be linked to the functional diversity of surrounding terrestrial ecosystems, with the strongest association occurring at several hundred meters and maximal spatial range to be 1.3–2.0 km upstream.

Furthermore, according to empirical variograms and fitted models, we found the effective range of spatial autocorrelation in terrestrial ecosystems to be 0.54–0.87 km (Fig. 3), which is smaller than the spatial range of the land-water linkage of biodiversity (1.3–2.0 km) discovered in this study. Moreover, there is no notable signal of spatial autocorrelation in our eDNA data (Fig. S8), and the observed spatial range of the land-water linkage of biodiversity is smaller than the pairwise distance of upstream nearest sites (mean: 3.54 km; min: 0.67 km; max: 6.01 km). Thus, the inherent spatial autocorrelation in the riverine network cannot drive the observed pattern, as it is at a different scale. As a consequence, we demonstrate that the spatial range of the land-water linkage of biodiversity is distinct, and it is not directly driven by spatial autocorrelation in either the riverine network or terrestrial ecosystems.

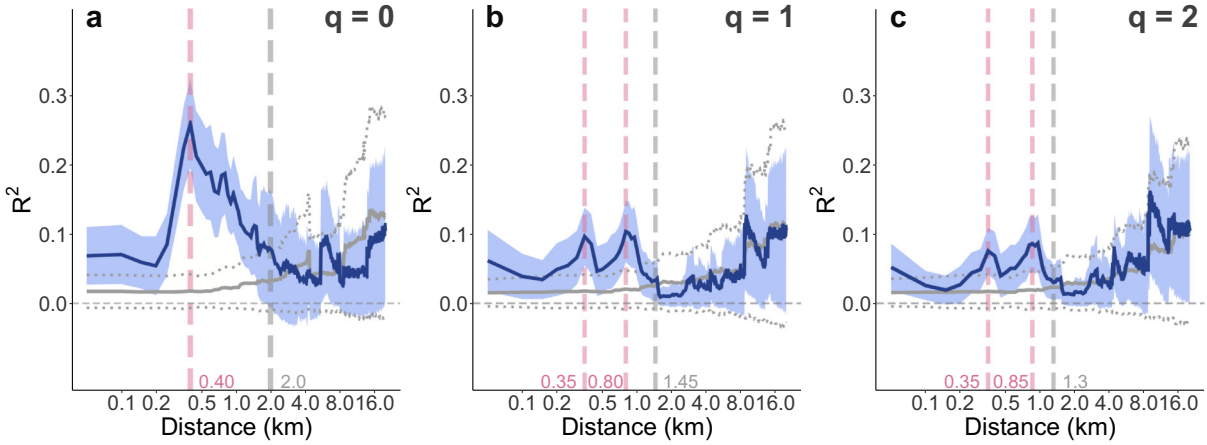

Fig. 5. Association between eDNA-derived biodiversity assessed in the river water and RS-derived terrestrial ecosystem functional diversity across increasing upstream distance in the Thur river catchment. The R^2 of the linear regression (blue lines, ± standard deviation given as light blue area) between eDNA-based Hill numbers with order **a**. q = 0 (equivalent to species richness), **b**. q = 1 (equivalent to the exponential of Shannon diversity), and **c**. q = 2 (equivalent to the inverse of Simpson index), and RS-based functional divergence (FDiv) across distance are given. As direct comparison, in grey lines the R^2 of the null models (± standard deviation, dotted lines) is shown.

Importantly, the unimodal or bimodal shape of the linkage of biodiversity is not caused by the variation of vegetation productivity, suggesting that the heterogeneity but not the productivity of terrestrial ecosystems contributes to local aquatic biodiversity. We tested this by firstly calculating the enhanced vegetation index (EVI) to represent vegetation productivity (Jiang et al., 2008). We adopted a type I ANOVA test to evaluate the relative contributions of EVI and FDiv to the Hill numbers across distance (Fig. 6). We found the F-value of FDiv was always higher than the F-value of EVI at distances smaller than maximal spatial range in both Test1 and Test2 (only parameter order is different), which indicates that FDiv rather than EVI better correlates with eDNA-derived biodiversity. In addition, we also found that EVI and FDiv were not correlated at distances <8.0 km (Fig. S10). Together, this evidences that the unimodal or bimodal signal of land-water linkage of biodiversity cannot be ascribed to the variation of vegetation productivity.

To disentangle the observed land-water linkage of biodiversity and to evaluate the possible contributions of direct and indirect effects, we mapped the ZOTUs against a customized MIDORI Reference 2 database for taxonomic information, which allowed us to identify the taxonomic affiliation and the possible origin of the most prominent ZOTUs and read numbers at phylum and class level, respectively (Fig. 7). Abundant affiliations both with respect to ZOTU richness and read numbers were found for Arthropods (especially Insecta), Ascomycota (a fungi phylum), and Bacillariophyta (diatoms). ZOTUs originated from organisms inhabiting both aquatic and terrestrial environments (Fig. 7), and most groups observed contain both aquatic and terrestrial taxa. Only a small portion (4 out of 44 classes) of ZOTUs came from organismal classes that were restricted to terrestrial ecosystems only, while 12 out of 44 classes were exclusively aquatic, indicating that the land-water linkage of biodiversity is not attributable to organismal migration across ecosystems (i.e., from terrestrial ecosystem to aquatic ecosystem), yet instead due to indirect effects of resource flows or trophic cascades. Then, we subsampled the eDNA data based on the taxonomic information to evaluate individual contributions across major taxonomic groups. Specifically, we calculated the relative abundances at the phylum level and assessed their associations with FDiv across distance. Among all the major taxonomic groups at the phylum level, we detected strong associations in Bacillariophyta, Chordata, Ascomycota, Cnidaria, Rotifera, Amoebozoa, Chlorophyta, Cryptophyta, and Porifera, although the spatial extents were varying (Fig. S11). Moreover, we repeated the same computation for terrestrial- or aquatic-only groups at the class level. Contrastingly, there was no apparent association between relative abundances with FDiv in terrestrial-only classes but some strong association patterns in aquatic-only classes (Fig. S12). Again, given the small portion in the total ZOTUs, terrestrial-only classes hardly contribute to the land-water linkage of biodiversity, substantiating that direct organismal migration is not a major mechanism. Hence, the indirect effects are the major factor in shaping the spatial fingerprint of land-water linkage of biodiversity. Importantly, these results also show that the land-water linkage of biodiversity includes contributions of aquatic and terrestrial origins, thus reflecting both an integrated signal of biodiversity across ecosystems and a signal of local ecosystem biodiversity.

4. Discussion

Combining eDNA sampling and multispectral remote sensing imagery, we demonstrated a spatial association of biodiversity between aquatic

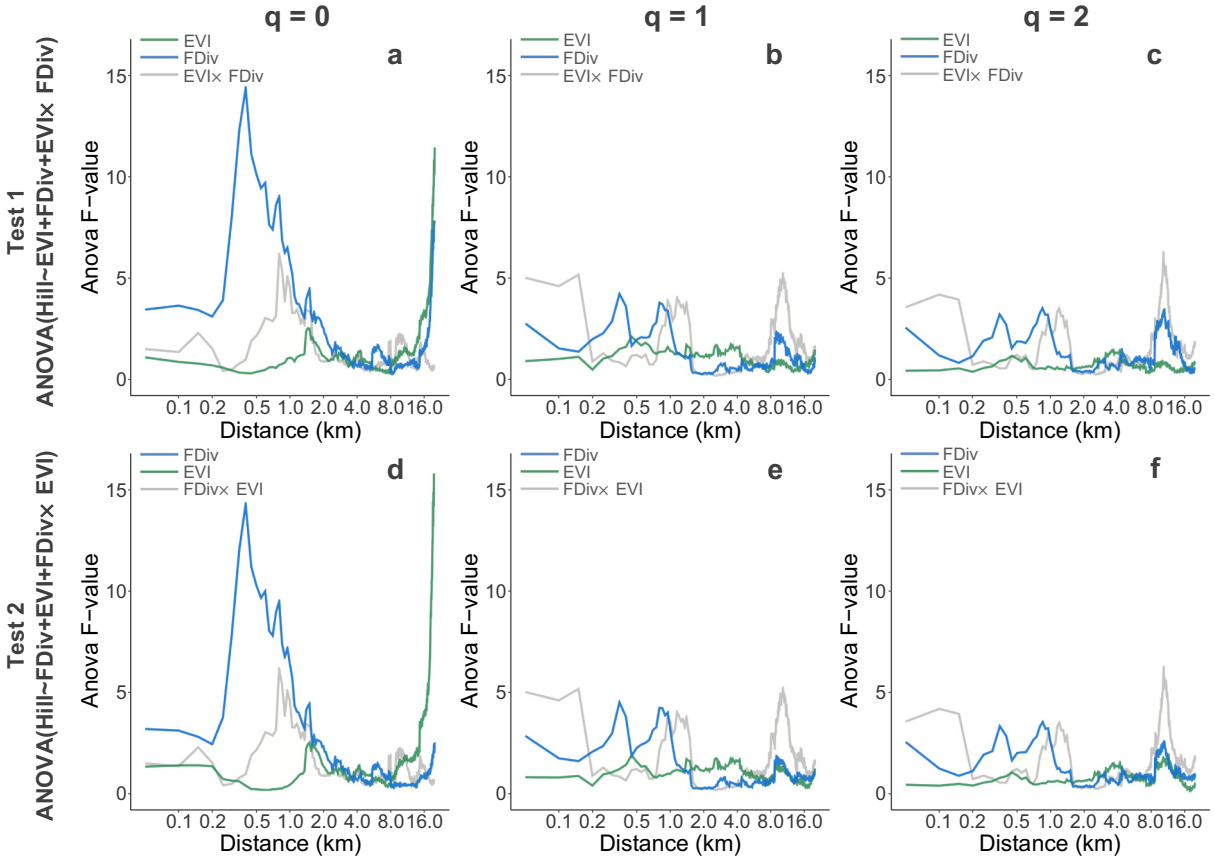

Fig. 6. Type I ANOVA test results of relative contributions of vegetation productivity (represented by the enhanced vegetation index, EVI) and terrestrial ecosystem functional diversity (represented by FDiv) to biodiversity patterns in the river (Hill number with orders q = 0, 1, 2) across distance. **a**. F-values of EVI, FDiv, and interaction term in Test 1 with Hill number order q = 0. **b**. F-values of EVI, FDiv, and interaction term in Test 1 with Hill number order q = 1. **c**. F-values of EVI, FDiv, and interaction term in Test 1 with Hill number order q = 2. **d**. F-values of EVI, FDiv, and interaction term in Test 2 with Hill number order q = 0. **e**. F-values of EVI, FDiv, and interaction term in Test 2 with Hill number order q = 1. **f**. F-values of EVI, FDiv, and interaction term in Test 2 with Hill number order q = 2.

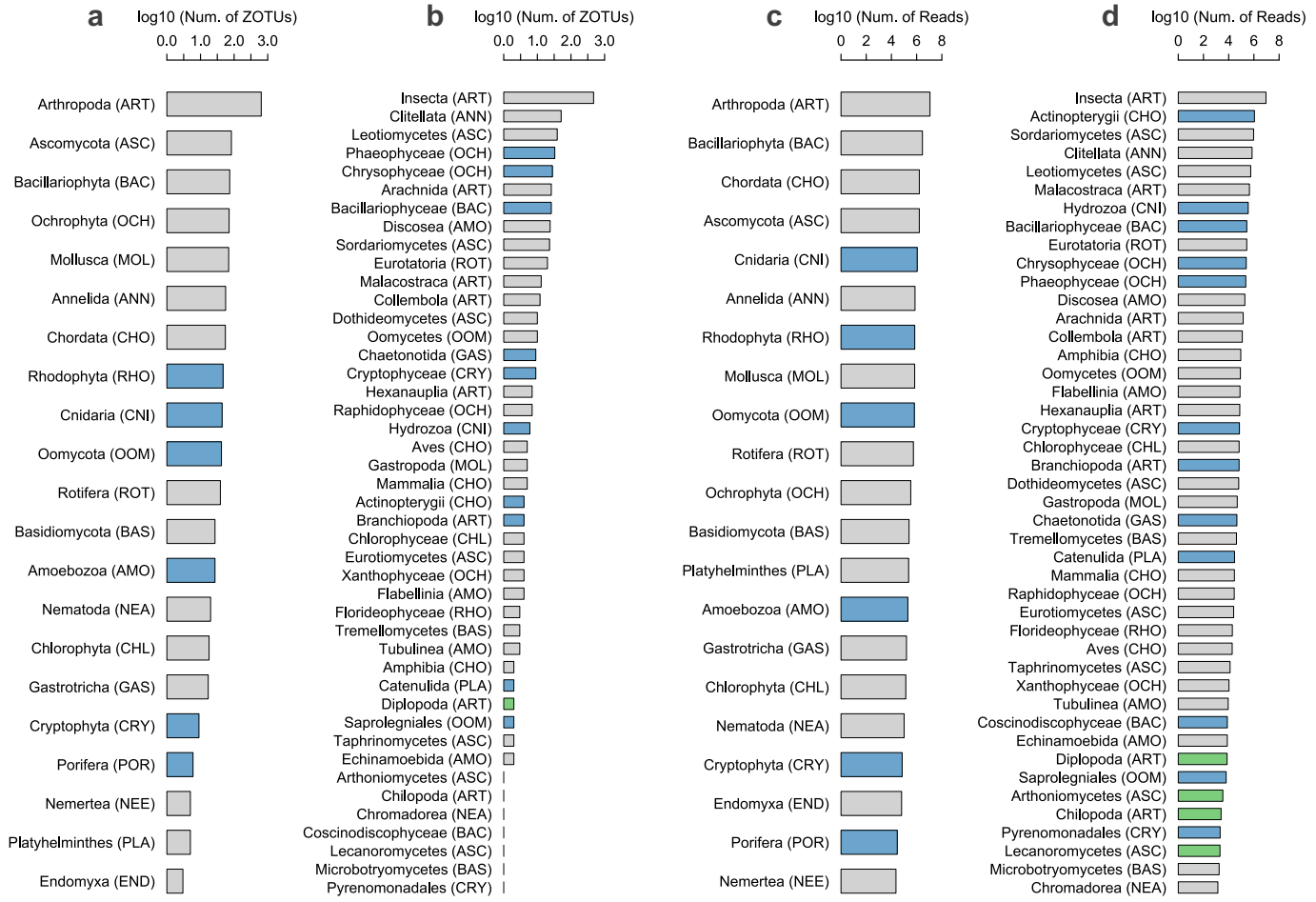

Fig. 7. Number of ZOTUs and reads in the eDNA data. **a**. Number of ZOTUs at the phylum level. **b**. Number of ZOTUs at the class level. **c**. Number of reads at the phylum level. **d**. Number of reads at the class level. ZOTUs with occurrences less than three at the phylum level were removed to avoid spurious effects. All numbers were log10-transformed before plotting. A three-letter code in the bracket after the taxonomic name indicates the phylum each class belongs to. The origin of taxonomic groups was marked with different colors: blue for aquatic origin only, green for terrestrial origin only, and grey for containing organisms inhabiting aquatic and/or terrestrial ecosystems. The taxonomic information of eDNA data indicates the land-water linkage of biodiversity is a signal from both aquatic and terrestrial origins.

and terrestrial ecosystems and gave a spatially explicit quantification of its peak strength, peaking across a catchment section at a 400 m radius upstream around the aquatic sampling site (Fig. 5). Overall, the signal of the land-water linkage of biodiversity covers a range of up to 2.0 km upstream, indicating that a place in a river and surrounding terrestrial ecosystems are closely interlinked, with a tight connection in terms of biodiversity. eDNA sampling data revealed indirect effects as the major contributing factor to this spatial association. Furthermore, for the first time, we provide a specific and scalable approach to quantify the spatial extent of such linkages across ecosystem types and identify a characteristic spatial land-water fingerprint.

The characterization of the terrestrial ecosystems from a biodiversity perspective was based on multiple physiological trait proxies (Fig. 3), capturing major components of the dominant vegetation cover. Contrary to traditional biodiversity surveys and estimates, which are often limited to small scales and numbers of sites and depend on specific taxonomic knowledge, our approach using high-resolution satellite RS data is not only capable of depicting regional and spatially continuous characteristics of biodiversity, but can be directly applied and scaled to map terrestrial biodiversity across all river catchments worldwide. Additionally, the characterization of aquatic biodiversity using eDNA allows a scaling across space and time, and most importantly, does not depend on prior knowledge on the occurrence of specific taxa. Thereby, this eDNA and RS combination approach could contribute to a global understanding of biodiversity patterns. Our method can, in principle, be applied and transferred to all land-water ecosystems worldwide, as it solely depends on broadly available RS data as well as eDNA water samples that can be taken across rivers from boreal to tropical ranges (Blackman et al., 2021; Zinger et al., 2020), and may be especially useful to uncover biodiversity patterns in understudied regions, such as regions beyond Europe and North America.

In this study, we identified a strong fingerprint of land-water linkage of biodiversity, with a metric of terrestrial ecosystem functional diversity developed on a combination of four physiological trait components of vegetation (Helfenstein et al., 2022). To evaluate the relative individual importance of these component proxies, namely CHL, CAR, ANT, and WAT, we removed one dimension at each time and repeated the calculation process. We found that the maximum values of R^2 dropped remarkably when CHL or WAT was removed (Fig. S13 & Table S1). Moreover, the shape was flatter after both CHL and WAT were removed (Fig. S14 & Table S1). This indicates that CHL and WAT, the indices inherently representing the photosynthesis activity of vegetation and thus carbon storage and potentially vegetation structure, mainly characterize the spatial fingerprint of land-water linkage of biodiversity.

For the characterization of the aquatic biodiversity (Fig. 4), we adopted a commonly used generic COI marker amplifying eDNA signals across a wide range of taxa. While it is predominantly used to target invertebrates, it also gives a high coverage of eukaryotic microorganisms (Zafeiropoulos et al., 2021). Consequently, a large proportion of retrieved sequences

aligned with macro-and micro-invertebrates; yet we also covered a wider breadth of taxa regarding ZOTUs, including microorganisms and vertebrates. The general validity of eDNA to reproduce overall biodiversity patterns is well established (Keck et al., 2022), and its use has been especially propagated for riverine systems (Altermatt et al., 2020; Blackman et al., 2021; Civade et al., 2016). More specifically, also for the specific study catchment of the river Thur, it has been shown how the eDNA method can accurately capture the biodiversity of Ephemeroptera, Plecoptera, and Trichoptera (EPT) (Mächler et al., 2019). Specifically the comparison to kicknet sampling and cumulative historical data (1981–2016) proved that eDNA metabarcoding (using the COI marker) captures the major components of diversity and, most importantly, can provide comparable data set for large sampling campaigns, and thus being suitable for eDNA based biodiversity assessments in general (Deiner et al., 2017; Mächler et al., 2021). In our eDNA data, 351 out of 1394 ZOTUs can be assigned at the species level, yet many of these taxa, as well as the un-assigned taxa, can reside in different ecosystems. Therefore, it is difficult to attribute most ZOTUs to exact either aquatic or terrestrial origins and the coverage of organisms is highly variable in the respective reference databases (Weigand et al., 2019). Therefore, to avoid any bias, we applied a taxonomy-free approach using ZOTUs only. This approach covers a broader taxonomic breadth yet does not address the contribution of individual taxonomic groups. Still, according to the taxonomic information and the origin of environments of our eDNA data (Fig. 7), we observed that ZOTUs originated from aquatic and terrestrial environments both contributed to the land-water linkage of biodiversity, and direct migration of terrestrial organisms was not a major contributing factor. We also evaluated the relative contribution of each of the major taxonomic groups at the phylum level to the spatial land-water fingerprint by omitting one of these major taxonomic groups at a time and repeating the calculations. Intriguingly, the association pattern was almost the same regardless of which taxonomic group was omitted (Fig. S15), suggesting that the land-water fingerprint of biodiversity is highly robust and thus does not depend on a single major organismal group.

Multiple expectations of possible mechanisms, which could be categorized as direct effects, such as organismal movement, and indirect effects, such as resource subsidies and food web interactions, have been proposed and thoroughly discussed in the cross-ecosystem and meta-ecosystem studies. Though focusing on different perspectives and being brought up individually, these possible mechanisms are basically mutually non-exclusive. In this study, we identified the origin of eDNA ZOTUs in the river at the phylum/class level, and evidenced that direct organismal movement was not a major contributing factor. Thus, it is more likely that the spatial fingerprint of land-water linkage of biodiversity is due to the indirect effects of resource subsidies or food web interactions at the spatial scale of 1.3–2.0 km upstream. The RS metric, FDiv, an index measuring the local diversity of ecosystem functioning and possible strength of within- or cross-ecosystem interactions, could better reflect the potential indirect effects from terrestrial ecosystems. Specifically, FDiv quantifies the heterogeneity of vegetation physiological trait distribution in terrestrial ecosystems within a distance buffer. Such local heterogeneity may cause spatial discrepancies in resources, or food web components in terrestrial ecosystems, then influence the biodiversity of aquatic ecosystems nearby. Nevertheless, it would go beyond our data to claim which of these processes is more prominent, as we cannot assign most of the ZOTUs at the species level, thereby limiting a functional understanding of aquatic communities. Therefore, we focused on documenting the specific spatial range of land-water linkage of biodiversity, while partitioning into very specific mechanisms would require a robust null model of how these mutually non-exclusive mechanisms may interfere.

The methodology to assess the spatial fingerprint of land-water linkage of biodiversity proved to be an efficient way to uncover an underlying picture of biodiversity in spatially coupled ecosystems, by combining in situ measures of eDNA and regional data of RS. Both eDNA metabarcoding and RS are capable of assessing biodiversity across scales because of easy access to vast quantities of information with high robustness and accuracy, non-invasive and standardized procedures, and relatively low costs (Kelly et al., 2014; Kissling et al., 2018; Skidmore et al., 2015; Valentini et al., 2016; Williams et al., 2021). Therefore, the methods applied here can contribute to next-generation biodiversity monitoring at regional to global scales (Bohan et al., 2017).

The spatial fingerprint of land-water linkage of biodiversity detected is robust and may be even more resolved when the spatio-temporal matching of the two approaches is increased. Our study adopted Sentinel-2 MSI Level-2A calibrated SR for RS measurements. It was generated on Level-1C top-of-atmosphere reflectance and is less affected by clouds or aerosols. Therefore, it is more accurate in mapping the physiological traits of vegetation. Due to the lack of Level-2A reflectance in 2016, we used Level-2A reflectance in 2017 for calculation in order to match the eDNA sampling at the respective seasonal time point. While there is likely seasonality in both RS and eDNA data (Bolton et al., 2020; De Souza et al., 2016), the inter-annual variation in RS between 2016 and 2017 is relatively minor, being testified by a very high correlation of corresponding bands and physiological trait indices on Level-1C data between 2016 and 2017 (Tables S2 & S3). Additionally, the meteorological conditions were very similar between 2016 and 2017, and both years were close to the normal condition in terms of temperature and precipitation (Table S4). Thus, the spatial fingerprint is robust across years, at least when the land cover and meteorological conditions are not changing. In reverse, the method may be directly applicable to detecting terrestrial ecosystem changes, as a change in the magnitude and extent of the spatial fingerprint may be expected.

Hitherto, biodiversity conservation and management have often been system specific, yet our work indicates strong cross-ecosystem dependencies at the spatial scale of hundreds of meters to a few kilometers. Consequently, our findings have direct implications. For example, the conservation buffer distance applied for streams or rivers in most countries is only a few to a few dozen meters. Given that we report spatial dependencies of 400 m to 2 km, our work suggests that managing biodiversity in aquatic systems requires the integration of terrestrial surroundings at such scales. Therefore, one direct conservation application could be an accurate measurement of conservation buffer distance across various catchments. Another direct implication is that the distances identified in our study can be used to determine protected area categories. For instance, buffer areas with a distance of 0–400 m to stream or river could be managed or protected more intensively, while buffer areas with a distance of 0.4–2.0 km to stream or river may need to be sustainably managed with respect to aquatic biodiversity effects. We note, however, that the scale of the spatial fingerprint could be catchment-specific, thus requiring a case-by-case evaluation in other parts of the world.

In conclusion, we uncovered a spatially explicit land-water linkage of biodiversity in a large mountainous catchment by using eDNA sampling and satellite remote sensing imagery. The linkage of biodiversity between rivers and surrounding terrestrial landscapes covers an area section of around 1.7 km^2 in the catchment with a radius of 2 km upstream, with the maximal strength at a radius of 400 m. This spatially explicit information identifies a characteristic fingerprint of land-water linkage of biodiversity in spatially coupled ecosystems. While developed in a mountainous region with different major land cover types, including forest, grassland, agriculture, and urban areas, our method does not depend on specific organismal groups, thus, can be used for all regions with spatially heterogeneous land cover types, providing an applicable basis for biodiversity conservation and land management in riverine systems globally.

CRediT authorship contribution statement

Heng Zhang: Conceptualization, Methodology, Software, Formal analysis, Writing – original draft. **Elvira Mächler:** Formal analysis, Investigation, Writing – review & editing. **Felix Morsdorf:** Methodology, Resources, Writing – review & editing. **Pascal A. Niklaus:** Methodology, Writing – review & editing. **Michael E. Schaepman:** Methodology, Resources, Writing – review & editing. **Florian Altermatt:** Conceptualization, Methodology, Resources, Writing – original draft, Supervision, Project administration, Funding acquisition.

Data availability

Data will be made available on request.

Declaration of competing interest

The authors declare that they have no known competing financial interests or personal relationships that could have appeared to influence the work reported in this paper.

Acknowledgements

We thank Chelsea Little for support during fieldwork, Luca Carraro for help extracting catchment information, and Isabelle Helfenstein and Enrico Bertuzzo for their help with functional divergence computation. Finally, we thank the reviewer for their helpful comments on our manuscript. F.A. is funded by the Swiss National Science Foundation Grants No 31003A_173074 and PP00P3_179089, and F.A, F.M., and M.S. by the University of Zurich Research Priority Programme on Global Change and Biodiversity (URPP GCB).

Appendix A. Supplementary data

Supplementary data to this article can be found online at https://doi.org/10.1016/j.scitotenv.2022.161365.

References

Alberdi, A., Gilbert, M.T.P., 2019. A guide to the application of hill numbers to DNA-based diversity analyses. Mol. Ecol. Resour. 19, 804–817.
Altermatt, F., Little, C.J., Mächler, E., Wang, S., Zhang, X., Blackman, R.C., 2020. Uncovering the complete biodiversity structure in spatial networks: the example of riverine systems. Oikos 129, 607–618.
Andrews, S., 2010. FastQC: a quality control tool for high throughput sequence data. Babraham Bioinformatics. Babraham Institute, Cambridge.
Bista, I., Carvalho, G.R., Walsh, K., Seymour, M., Hajibabaei, M., Lallias, D., Christmas, M., Creer, S., 2017. Annual time-series analysis of aqueous eDNA reveals ecologically relevant dynamics of lake ecosystem biodiversity. Nat. Commun. 8, 14087.
Blackman, R.C., Osathanunkul, M., Brantschen, J., Di Muri, C., Harper, L.R., Mächler, E., Hänfling, B., Altermatt, F., 2021. Mapping biodiversity hotspots of fish communities in subtropical streams through environmental DNA. Sci. Rep. 11, 10375.
Blowes, S.A., Supp, S.R., Antão, L.H., Bates, A., Bruelheide, H., Chase, J.M., Moyes, F., Magurran, A., McGill, B., Myers-Smith, I.H., 2019. The geography of biodiversity change in marine and terrestrial assemblages. Science 366, 339–345.
Bohan, D.A., Vacher, C., Tamaddoni-Nezhad, A., Raybould, A., Dumbrell, A.J., Woodward, G., 2017. Next-generation global biomonitoring: large-scale, automated reconstruction of ecological networks. Trends Ecol. Evol. 32, 477–487.
Bohmann, K., Evans, A., Gilbert, M.T.P., Carvalho, G.R., Creer, S., Knapp, M., Douglas, W.Y., De Bruyn, M., 2014. Environmental DNA for wildlife biology and biodiversity monitoring. Trends Ecol. Evol. 29, 358–367.
Bolton, D.K., Gray, J.M., Melaas, E.K., Moon, M., Eklundh, L., Friedl, M.A., 2020. Continental-scale land surface phenology from harmonized landsat 8 and Sentinel-2 imagery. Remote Sens. Environ. 240, 111685.
Bush, A., Sollmann, R., Wilting, A., Bohmann, K., Cole, B., Balzter, H., Martius, C., Zlinszky, A., Calvignac-Spencer, S., Cobbold, C.A., 2017. Connecting earth observation to high-throughput biodiversity data. Nat. Ecol. Evol. 1, 0176.
Carraro, L., Mächler, E., Wüthrich, R., Altermatt, F., 2020. Environmental DNA allows upscaling spatial patterns of biodiversity in freshwater ecosystems. Nat. Commun. 11, 3585.
Cilleros, K., Valentini, A., Allard, L., Dejean, T., Etienne, R., Grenouillet, G., Iribar, A., Taberlet, P., Vigouroux, R., Brosse, S., 2019. Unlocking biodiversity and conservation studies in high-diversity environments using environmental DNA (eDNA): a test with guianese freshwater fishes. Mol. Ecol. Resour. 19, 27–46.
Civade, R., Dejean, T., Valentini, A., Roset, N., Raymond, J.-C., Bonin, A., Taberlet, P., Pont, D., 2016. Spatial representativeness of environmental DNA metabarcoding signal for fish biodiversity assessment in a natural freshwater system. PloS one 11, e0157366.
Dahlin, K.M., Zarnetske, P.L., Read, Q.D., Twardochleb, L.A., Kamoske, A.G., Cheruvelil, K.S., Soranno, P.A., 2021. Linking terrestrial and aquatic biodiversity to ecosystem function across scales, trophic levels, and realms. Front. Environ. Sci. 9, 217.
De Souza, L.S., Godwin, J.C., Renshaw, M.A., Larson, E., 2016. Environmental DNA (eDNA) detection probability is influenced by seasonal activity of organisms. PloS one 11, e0165273.
Deiner, K., Bik, H.M., Mächler, E., Seymour, M., Lacoursière-Roussel, A., Altermatt, F., Creer, S., Bista, I., Lodge, D.M., De Vere, N., 2017. Environmental DNA metabarcoding: transforming how we survey animal and plant communities. Mol. Ecol. 26, 5872–5895.
Deiner, K., Fronhofer, E.A., Mächler, E., Walser, J.-C., Altermatt, F., 2016. Environmental DNA reveals that rivers are conveyer belts of biodiversity information. Nat. Commun. 7, 12544.
Díaz, S., Kattge, J., Cornelissen, J.H., Wright, I.J., Lavorel, S., Dray, S., Reu, B., Kleyer, M., Wirth, C., Prentice, I.C., 2016. The global spectrum of plant form and function. Nature 529, 167–171.
Drusch, M., Del Bello, U., Carlier, S., Colin, O., Fernandez, V., Gascon, F., Hoersch, B., Isola, C., Laberinti, P., Martimort, P., 2012. Sentinel-2: ESA's optical high-resolution mission for GMES operational services. Remote Sens. Environ. 120, 25–36.
Dudgeon, D., 2019. Multiple threats imperil freshwater biodiversity in the anthropocene. Curr. Biol. 29, R960–R967.
Fahey, R.T., Atkins, J.W., Gough, C.M., Hardiman, B.S., Nave, L.E., Tallant, J.M., Nadehoffer, K.J., Vogel, C., Scheuermann, C.M., Stuart-Haëntjens, E., 2019. Defining a spectrum of integrative trait-based vegetation canopy structural types. Ecol. Lett. 22, 2049–2059.
Gonzalez, A., Germain, R.M., Srivastava, D.S., Filotas, E., Dee, L.E., Gravel, D., Thompson, P.L., Isbell, F., Wang, S., Kéfi, S., 2020. Scaling-up biodiversity-ecosystem functioning research. Ecol. Lett. 23, 757–776.
Gorelick, N., Hancher, M., Dixon, M., Ilyushchenko, S., Thau, D., Moore, R., 2017. Google earth engine: planetary-scale geospatial analysis for everyone. Remote Sens. Environ. 202, 18–27.
Gounand, I., Harvey, E., Little, C.J., Altermatt, F., 2018a. Meta-ecosystems 2.0: rooting the theory into the field. Trends Ecol. Evol. 33, 36–46.
Gounand, I., Little, C.J., Harvey, E., Altermatt, F., 2018b. Cross-ecosystem carbon flows connecting ecosystems worldwide. Nat. Commun. 9, 4825.
Gravel, D., Guichard, F., Loreau, M., Mouquet, N., 2010. Source and sink dynamics in meta-ecosystems. Ecology 91, 2172–2184.
Grimm, N.B., Gergel, S.E., McDowell, W.H., Boyer, E.W., Dent, C.L., Groffman, P., Hart, S.C., Harvey, J., Johnston, C., Mayorga, E., 2003. Merging aquatic and terrestrial perspectives of nutrient biogeochemistry. Oecologia 137, 485–501.
Guichard, F., Marleau, J., 2021. Meta-ecosystem dynamics. Springer, Cham.
Helfenstein, I.S., Schneider, F.D., Schaepman, M.E., Morsdorf, F., 2022. Assessing biodiversity from space: impact of spatial and spectral resolution on trait-based functional diversity. Remote Sens. Environ. 275, 113024.
Hill, M.O., 1973. Diversity and evenness: a unifying notation and its consequences. Ecology 54, 427–432.
Hughes, A.C., Orr, M.C., Yang, Q., Qiao, H., 2021. Effectively and accurately mapping global biodiversity patterns for different regions and taxa. Glob. Ecol. Biogeogr. 30, 1375–1388.
Jetz, W., Cavender-Bares, J., Pavlick, R., Schimel, D., Davis, F.W., Asner, G.P., Guralnick, R., Kattge, J., Latimer, A.M., Moorcroft, P., 2016. Monitoring plant functional diversity from space. Nat. Plants 2, 16024.
Jiang, Z., Huete, A.R., Didan, K., Miura, T., 2008. Development of a two-band enhanced vegetation index without a blue band. Remote Sens. Environ. 112, 3833–3845.
Jost, L., 2007. Partitioning diversity into independent alpha and beta components. Ecology 88, 2427–2439.
Keck, F., Blackman, R.C., Bossart, R., Brantschen, J., Couton, M., Hürlemann, S., Kirschner, D., Locher, N., Zhang, H., Altermatt, F., 2022. Meta-analysis shows both congruence and complementarity of DNA and eDNA metabarcoding to traditional methods for biological community assessment. Mol. Ecol. 31, 1820–1835.
Kelly, R.P., Port, J.A., Yamahara, K.M., Martone, R.G., Lowell, N., Thomsen, P.F., Mach, M.E., Bennett, M., Prahler, E., Caldwell, M.R., 2014. Harnessing DNA to improve environmental management. Science 344, 1455–1456.
Kennedy, C.M., Oakleaf, J.R., Theobald, D.M., Baruch-Mordo, S., Kiesecker, J., 2019. Managing the middle: a shift in conservation priorities based on the global human modification gradient. Glob. Chang. Biol. 25, 811–826.
Kissling, W.D., Ahumada, J.A., Bowser, A., Fernandez, M., Fernández, N., García, E.A., Guralnick, R.P., Isaac, N.J., Kelling, S., Los, W., 2018. Building essential biodiversity variables (EBVs) of species distribution and abundance at a global scale. Biol. Rev. 93, 600–625.
Kraft, N.J., Comita, L.S., Chase, J.M., Sanders, N.J., Swenson, N.G., Crist, T.O., Stegen, J.C., Vellend, M., Boyle, B., Anderson, M.J., 2011. Disentangling the drivers of β diversity along latitudinal and elevational gradients. Science 333, 1755–1758.
Lausch, A., Bastian, O., Klotz, S., Leitão, P.J., Jung, A., Rocchini, D., Schaepman, M.E., Skidmore, A.K., Tischendorf, L., Knapp, S., 2018. Understanding and assessing vegetation health by in situ species and remote-sensing approaches. Methods Ecol. Evol. 9, 1799–1809.
Leray, M., Yang, J.Y., Meyer, C.P., Mills, S.C., Agudelo, N., Ranwez, V., Boehm, J.T., Machida, R.J., 2013. A new versatile primer set targeting a short fragment of the mitochondrial COI region for metabarcoding metazoan diversity: application for characterizing coral reef fish gut contents. Front. Zool. 10, 34.
Leroux, S.J., Loreau, M., 2008. Subsidy hypothesis and strength of trophic cascades across ecosystems. Ecol. Lett. 11, 1147–1156.
Lin, M., Simons, A.L., Harrigan, R.J., Curd, E.E., Schneider, F.D., Ruiz-Ramos, D.V., Gold, Z., Osborne, M.G., Shirazi, S., Schweizer, T.M., 2021. Landscape analyses using eDNA metabarcoding and earth observation predict community biodiversity in California. Ecol. Appl. 31, e02379.
Lodge, D.M., Turner, C.R., Jerde, C.L., Barnes, M.A., Chadderton, L., Egan, S.P., Feder, J.L., Mahon, A.R., Pfrender, M.E., 2012. Conservation in a cup of water: estimating biodiversity and population abundance from environmental DNA. Mol. Ecol. 21, 2555–2558.
Loreau, M., Mouquet, N., Holt, R.D., 2003. Meta-ecosystems: a theoretical framework for a spatial ecosystem ecology. Ecol. Lett. 6, 673–679.
Mächler, E., Little, C.J., Wüthrich, R., Alther, R., Fronhofer, E.A., Gounand, I., Harvey, E., Hürlemann, S., Walser, J.C., Altermatt, F., 2019. Assessing different components of diversity across a river network using eDNA. Environ. DNA 1, 290–301.
Mächler, E., Walser, J.-C., Altermatt, F., 2021. Decision-making and best practices for taxonomy-free environmental DNA metabarcoding in biomonitoring using hill numbers. Mol. Ecol. 30, 3326–3339.

Matheron, G., 1963. Principles of geostatistics. Econ. Geol. 58, 1246–1266.
Mittermeier, R.A., Turner, W.R., Larsen, F.W., Brooks, T.M., Gascon, C., 2011. Global biodiversity conservation: the critical role of hotspots. Biodiversity Hotspots. Springer, Berlin, Heidelberg, Heidelberg, pp. 3–22.
Nakano, S., Murakami, M., 2001. Reciprocal subsidies: dynamic interdependence between terrestrial and aquatic food webs. Proc. Natl. Acad. Sci. 98, 166–170.
O'Connor, B., Bojinski, S., Röösli, C., Schaepman, M.E., 2020. Monitoring global changes in biodiversity and climate essential as ecological crisis intensifies. Eco. Inform. 55, 101033.
Oehri, J., Schmid, B., Schaepman-Strub, G., Niklaus, P.A., 2020. Terrestrial land-cover type richness is positively linked to landscape-level functioning. Nat. Commun. 11, 154.
Pereira, H.M., Ferrier, S., Walters, M., Geller, G.N., Jongman, R., Scholes, R.J., Bruford, M.W., Brummitt, N., Butchart, S., Cardoso, A., 2013. Essential biodiversity variables. Science 339, 277–278.
Pimm, S.L., Jenkins, C.N., Abell, R., Brooks, T.M., Gittleman, J.L., Joppa, L.N., Raven, P.H., Roberts, C.M., Sexton, J.O., 2014. The biodiversity of species and their rates of extinction, distribution, and protection. Science 344, 1246752.
Polis, G.A., Anderson, W.B., Holt, R.D., 1997. Toward an integration of landscape and food web ecology: the dynamics of spatially subsidized food webs. Annu. Rev. Ecol. Syst. 28, 289–316.
Pont, D., Rocle, M., Valentini, A., Civade, R., Jean, P., Maire, A., Roset, N., Schabuss, M., Zornig, H., Dejean, T., 2018. Environmental DNA reveals quantitative patterns of fish biodiversity in large rivers despite its downstream transportation. Sci. Rep. 8, 10361.
Rodriguez-Iturbe, I., Rinaldo, A., 2001. Fractal River Basins: Chance and Self-organization. Cambridge University Press, Cambridge.
Schmitz, O.J., Wilmers, C.C., Leroux, S.J., Doughty, C.E., Atwood, T.B., Galetti, M., Davies, A.B., Goetz, S.J., 2018. Animals and the zoogeochemistry of the carbon cycle. Science 362, eaar3213.
Schneider, F.D., Morsdorf, F., Schmid, B., Petchey, O.L., Hueni, A., Schimel, D.S., Schaepman, M.E., 2017. Mapping functional diversity from remotely sensed morphological and physiological forest traits. Nat. Commun. 8, 1441.
Shackleton, M., Rees, G.N., Watson, G., Campbell, C., Nielsen, D., 2019. Environmental DNA reveals landscape mosaic of wetland plant communities. Glob. Ecol. Conerv. 19, e00689.
Shogren, A.J., Tank, J.L., Andruszkiewicz, E., Olds, B., Mahon, A.R., Jerde, C.L., Bolster, D., 2017. Controls on eDNA movement in streams: transport, retention, and resuspension. Sci. Rep. 7, 5065.
Sims, D.A., Rahman, A.F., Cordova, V.D., El-Masri, B.Z., Baldocchi, D.D., Flanagan, L.B., Goldstein, A.H., Hollinger, D.Y., Misson, L., Monson, R.K., 2006. On the use of MODIS EVI to assess gross primary productivity of North American ecosystems. 111, G04015.
Skidmore, A.K., Coops, N.C., Neinavaz, E., Ali, A., Schaepman, M.E., Paganini, M., Kissling, W.D., Vihervaara, P., Darvishzadeh, R., Feilhauer, H., 2021. Priority list of biodiversity metrics to observe from space. Nat. Ecol. Evol. 5, 896–906.
Skidmore, A.K., Pettorelli, N., Coops, N.C., Geller, G.N., Hansen, M., Lucas, R., Mücher, C.A., O'Connor, B., Paganini, M., Pereira, H.M., Schaepman, M.E., Turner, W., Wang, T., Wegmann, M., 2015. Agree on biodiversity metrics to track from space: ecologists and space agencies must forge a global monitoring strategy. Nature 523, 403–406.
Soininen, J., Bartels, P., Heino, J., Luoto, M., Hillebrand, H., 2015. Toward more integrated ecosystem research in aquatic and terrestrial environments. Bioscience 65, 174–182.
Taberlet, P., Coissac, E., Pompanon, F., Brochmann, C., Willerslev, E., 2012. Towards next-generation biodiversity assessment using DNA metabarcoding. Mol. Ecol. 21, 2045–2050.
Thompson, P.L., Kéfi, S., Zelnik, Y.R., Dee, L.E., Wang, S., de Mazancourt, C., Loreau, M., Gonzalez, A., 2021. Scaling up biodiversity–ecosystem functioning relationships: the role of environmental heterogeneity in space and time. Proc. R. Soc. B 288, 20202779.
Thomsen, P.F., Willerslev, E., 2015. Environmental DNA–An emerging tool in conservation for monitoring past and present biodiversity. Biol. Conserv. 183, 4–18.
Turak, E., Harrison, I., Dudgeon, D., Abell, R., Bush, A., Darwall, W., Finlayson, C.M., Ferrier, S., Freyhof, J., Hermoso, V., 2017. Essential biodiversity variables for measuring change in global freshwater biodiversity. Biol. Conserv. 213, 272–279.
Valentini, A., Taberlet, P., Miaud, C., Civade, R., Herder, J., Thomsen, P.F., Bellemain, E., Besnard, A., Coissac, E., Boyer, F., 2016. Next-generation monitoring of aquatic biodiversity using environmental DNA metabarcoding. Mol. Ecol. 25, 929–942.
Villéger, S., Mason, N.W., Mouillot, D., 2008. New multidimensional functional diversity indices for a multifaceted framework in functional ecology. Ecology 89, 2290–2301.
Visco, J.A., Apothéloz-Perret-Gentil, L., Cordonier, A., Esling, P., Pillet, L., Pawlowski, J., 2015. Environmental monitoring: inferring the diatom index from next-generation sequencing data. Environ. Sci. Technol. 49, 7597–7605.
Ward, J., Tockner, K., Arscott, D.B., Claret, C., 2002. Riverine landscape diversity. Freshw. Biol. 47, 517–539.
Weigand, H., Beermann, A.J., Čiampor, F., Costa, F.O., Csabai, Z., Duarte, S., Geiger, M.F., Grabowski, M., Rimet, F., Rulik, B., 2019. DNA barcode reference libraries for the monitoring of aquatic biota in Europe: gap-analysis and recommendations for future work. Sci. Total Environ. 678, 499–524.
Williams, L.J., Cavender-Bares, J., Townsend, P.A., Couture, J.J., Wang, Z., Stefanski, A., Messier, C., Reich, P.B., 2021. Remote spectral detection of biodiversity effects on forest biomass. Nat. Ecol. Evol. 5, 46–54.
Yamasaki, E., Altermatt, F., Cavender-Bares, J., Schuman, M.C., Zuppinger-Dingley, D., Garonna, I., Schneider, F.D., Guillén-Escribà, C., van Moorsel, S.J., Hahl, T., 2017. Genomics meets remote sensing in global change studies: monitoring and predicting phenology, evolution and biodiversity. Curr. Opin. Environ. Sustain. 29, 177–186.
Zafeiropoulos, H., Gargan, L., Hintikka, S., Pavloudi, C., Carlsson, J., 2021. The dark mAtteR iNvestigator (DARN) tool: getting to know the known unknowns in COI amplicon data. Metabarcoding Metagenom. 5, e69657.
Zheng, Z., Zeng, Y., Schneider, F.D., Zhao, Y., Zhao, D., Schmid, B., Schaepman, M.E., Morsdorf, F., 2020. Mapping functional diversity using individual tree-based morphological and physiological traits in a subtropical forest. Remote Sens. Environ. 252, 112170.
Zinger, L., Donald, J., Brosse, S., Gonzalez, M.A., Iribar, A., Leroy, C., Murienne, J., Orivel, J., Schimann, H., Taberlet, P., 2020. Advances and prospects of environmental DNA in neotropical rainforests. Adv. Ecol. Res. 62, 331–373.